ADVANCED FUNCTIONAL MATERIALS
www.afm-journal.de

Three Dimensional Graphene Foam/Polymer Hybrid as a High Strength Biocompatible Scaffold

*Andy Nieto, Rupak Dua, Cheng Zhang, Benjamin Boesl, Sharan Ramaswamy, and Arvind Agarwal**

Graphene foam (GrF)/polylactic acid–poly-ε-caprolactone copolymer (PLC) hybrid (GrF-PLC) scaffold is synthesized in order to utilize both the desirable properties of graphene and that of foams such as excellent structural characteristics and a networked 3-D structure for cells to proliferate in. The hybrid scaffold is synthesized by a dip-coating method that enables retention of the porous 3D structure. The excellent wettability of PLC with graphene foam along with the formation of PLC bridges leads to a ≈3700% enhancement in strength and a ≈3100% increase in ductility in the GrF-PLC scaffold. Biocompatibility of both graphene foam and GrF-PLC scaffold is demonstrated by culturing of human mesenchymal stem cells (hMSCs) for 28 days, a period over which cell proliferation is robust. The hMSCs are differentiated in chondrogenic media and supported chondrogenesis in both scaffolds. The demand for aggrecan extracellular matrix protein synthesis is reduced in hybrids due to improved bearing of cell-induced loads, this may be critical for ensuring adequate cellular distribution and layering of extracellular matrix. Hence, the unique mechanical and biotolerant properties of the GrF-PLC scaffold are suited for musculoskeletal tissue engineering applications, such as the growth of de novo cartilage to replace cartilage lost due to injury or osteoarthritis.

1. Introduction

Graphene is a 2-D layer of sp^2 bonded carbon atoms that has attracted interest in nearly all fields of materials science because of its excellent electrical,[1–4] thermal,[1,5] and mechanical properties.[1,3,6–9] Graphene has extraordinary mechanical properties such as high elastic modulus (1 TPa[7]) and yield strength (≈130 GPa[6]) which have been utilized in polymer, metal, and ceramic matrix composites in order to enhance their mechanical performance. One of the critical challenges for effective graphene-based composites is the uniform distribution of graphene in the composite matrix. The effective dispersion of graphene has been the subject of significant research, with the most effective methods being limited by material systems or cost. The recent development of 3-D graphene foams (GrF)[10–29] represents a solution for providing uniform distributions of graphene in composites. 3-D graphene foams form an interconnected continuous network of graphene thus eliminating the need for expensive and/or ineffective dispersion methods.

In this study we propose the use of a 3-D graphene foam/polymer composite as a flexible high strength biocompatible scaffolding material for tissue engineering purposes. Graphene has been shown to be a biocompatible material in recent studies.[30–32] Human stem cells (neural and mesenchymal) survive and experience accelerated differentiation on a graphene surface. While several studies[11–16,23,27,28] have utilized the high surface area and macroporous structure of 3-D graphene foam-based composites for energy storage applications, only a few studies to date[25,33] have exploited the inherent advantages of this unique structure for cell support, proliferation, and extracellular matrix (ECM) deposition. Studies on the biocompatibility of 3-D graphene foams have found that neural stem cells (NSCs) successfully proliferated and differentiated on the 3-D graphene structure. The porous 3-D graphene structure provides a microenvironment for the cells to grow within a 3-D biomimetic framework, while simultaneously enhancing the functionality of the electro-active neural cells by providing highly conductive pathways for charge transport.[33] Furthermore, 3-D graphene foams cultured with microglial cells exhibited anti-inflammatory behavior not seen in 2-D graphene foams.[25] A few recent studies have also investigated the mechanical properties of graphene foam reinforced polymer composites.[34–37] Graphene foam/polymer composites exhibit superb flexibility as evidenced by their recovery after compressive strains of up to 80%[36,37] and cyclic bending tests of nearly 180°.[34] The

A. Nieto, C. Zhang, Prof. B. Boesl, Prof. A. Agarwal
Nanomechanics and Nanotribology Laboratory
Mechanical and Materials Engineering
Florida International University
Miami, FL 33174, USA
E-mail: agarwala@fiu.edu
A. Nieto
Department of Chemical Engineering and Materials Science
One Shields Avenue
University of California Davis
Davis, CA 95616, USA
Dr. R. Dua, Prof. S. Ramaswamy
Biomedical Engineering
Florida International University
10555 West Flagler Street, EC 3464, USA

DOI: 10.1002/adfm.201500876

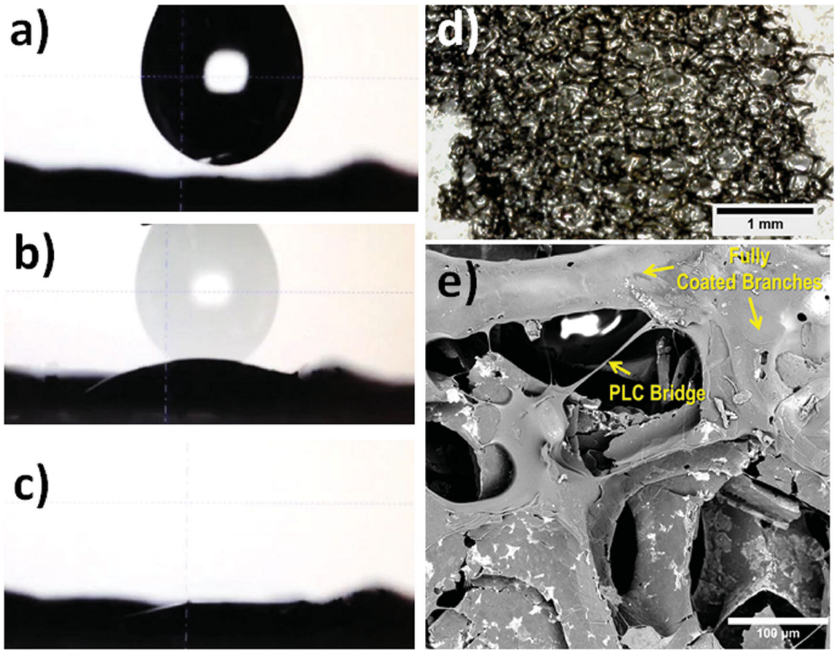

Figure 1. a) Image sequence of contact angle test before droplet contacts the surface. b) Single frame captures both the droplet as it approaches the foam and then rapidly spreads throughout the foam surface. c) Droplet forms near zero contact angle hence demonstrating near perfect wetting. d) Optical image of GrF-PLC hybrid scaffold. e) SEM image of GrF-PLC structure, thin strands of PLC can be seen to formed bridges throughout the sample. Retention of 3D porous structure can be seen in both optical and SEM images.

enhancement of toughness, ductility, and tensile strength[35] in graphene foam/polymer composites is especially noteworthy as their ultra-low density (≈0.005 g cm^{-3}) yield exceptional specific properties.

We focus specifically on the need for high strength biocompatible scaffolding materials for musculoskeletal regenerative applications related to cartilage loss and/or deterioration. Graphene provides many of the properties desirable in a scaffold for de novo cartilage growth. The scaffold must be able to effectively transfer loads to the surrounding joints and bone;[38] the high surface area of graphene foam enables effective transfer of loads in composites.[39–42] Viscoelasticity is needed in cartilage scaffolding in order to provide flexibility and damping of loads; graphene has been shown to have excellent damping properties[43] that can be effectively utilized in a composite material.[44] A lubricated surface is also desirable as the wear of cartilage ultimately causes osteoarthritis and the associated pain; graphene is a solid state lubricant and can effectively enhance tribological properties of composites.[40,45] Finally, a cartilage scaffold must be biocompatible in order to prevent infection or rejection by the native tissue; graphene has been shown to be biocompatible[25,30–32] and it is used in the present work in conjunction with the biodegradable polymer PLC (a copolymer of polylactic acid and poly-ε-caprolactone).[46] Several current works in cartilage tissue engineering make use of hydrogel-based scaffolds.[47–50] Notably, while hydrogels promote cell proliferation and tissue repair, they do not provide the structure to enable systematic distribution of cellular and ECM components. While graphene itself is not degradable within the composite, we hypothesized that the sustained presence of graphene after degradation of PLC will continue to support layered ECM deposition in a controlled manner, if interpenetrating networks present within the original composite material can guide initial tissue framework. These tissue remodeling events are crucial for long-term success of the procedure.

In this work, we synthesize a 3D graphene foam/PLC hybrid (GrF-PLC). The foam structure intrinsically facilitates interpenetrating networks between graphene and PLC, in order to promote cell distribution and ECM layering within the construct. We utilize a simple dip coating method for the GrF-PLC fabrication; the coating time is optimized to ensure retention of a porous foam structure. Wetting angle measurements are conducted to demonstrate the effectiveness of the PLC coating. Mechanical properties of the GrF-PLC hybrid are evaluated in tension and compression at multiple length scales using nanoindentation and in situ tensile testing inside scanning electron microscope. Cell seeding in the GrF-PLC scaffold environment is evaluated using human mesenchymal stem cells (hMSCs) on the scaffold, which has shown to be a promising cell source for cartilage tissue engineering in several studies.[47,51] Specifically, the suitability of the GrF-PLC scaffold for musculoskeletal tissue engineering applications, specifically for cartilage, is evaluated by culturing the hMSCs in a chondrogenic media, while phenotype is evaluated by immunostaining after 28 days.

2. Results and Discussion

2.1. Synthesis

The 3-D graphene foam (Graphene Laboratories, Calverton, NY, USA) used in this study was synthesized by chemical vapor deposition (CVD) growth of graphene on a Ni foam template, followed by an etching step to dissolve the Ni structure. The graphene foam has an ultralow density of 0.005 g cm^{-3} (0.002 relative density) and consists of large macroscale open pores typically 100–200 µm in diameter and 50–80 µm thick foam walls.[52] It was desired for the scaffold composite to retain this porous, high surface area structure and hence only a thin layer of PLC reinforcement was permissible. Graphene foams are known to be hydrophobic,[24] as verified by water wetting angles measurements (Supporting Information, Figure S1); such poor wettability is detrimental to obtaining a thin coating. By contrast, wetting angle measurements shown in **Figure 1**a–c revealed that PLC has near perfect wetting with the graphene foam. The drops of PLC instantaneously spread out over the graphene foam, indicating a wetting angle of ≈0°. This excellent wetting allows the PLC to cover the graphene foam with only a very thin layer. The PLC layer will therefore not aggregate and

Table 1. Summary of Graphene Foam/PLC scaffold mechanical properties in compression and tension.

Compression				
Experimental method	Elastic modulus [MPa]	Strain to failure [%]	Hardness [kPa]	Bulk foam elastic modulus (calculated by Equation (1)) [Pa]
Nanoindentation	3.6 ± 0.3	–	69.8 ± 5.7	17.6 ± 1.2
Tension				
Experimental method	Elastic modulus [kPa]	Strain to failure [%]	Ultimate tensile strength (UTS) [kPa]	Foam wall elastic modulus (calculated by Equation (1)) [GPa]
Tensile testing	254.0 ± 43.7	276.3 ± 65.3	184 ± 48.1	52.35 ± 9.0

increase in thickness until the graphene foam surface is fully saturated; this allows the macroporous high surface area structure to be retained.

The graphene foam/PLC (GrF-PLC) hybrids were prepared by a simple dip coating method where the PLC polymer is synthesized in a solution of acetone in which the graphene foam is then dipped for a controlled period of time. The PLC polymer coated on the graphene foam undergoes the final steps of polymerization (i.e., solidification), while in contact with the graphene foam and hence a high strength bond is formed between the graphene foam and PLC in the resulting hybrid structure. The dipping time was optimized to prevent oversaturation of the graphene foam and hence retain the macroporous structure. The evaluation of graphene foam saturation was done using scanning electron microscopy (SEM). SEM images for dipping times of 30 and 120 s are provided in Supporting Information, Figure S2. These times were excessive and resulted in the foam becoming fully embedded in the PLC matrix which results in the loss of the macroporous structure desired for cell proliferation.

The optimum dipping time was found to be 5 s and resulted in the GrF-PLC hybrid structure shown in Figure 1d,e. The dipping time of 5 s resulted in a thin PLC layer over the majority of the interpenetrating networks of foam branches as seen in Figure 1e. The large graphene foam pores are not filled with PLC as with the previous cases, instead strands of PLC can be seen forming interconnected structures between branches of graphene foam. The thickness of the coating is not homogenous as seen in Figure 1e; however strands of PLC that span some of the macropores in the graphene foam have diameters of ≈10 µm. These strands form as the PLC coating extends beyond branches and across the macropores and thereby provides an estimate of the length scale of the coating thickness. The amount of PLC added was not sufficient to obtain a measureable change in the density of 3D graphene foam which was measured using a helium pycnometer.

2.2. Strengthening Mechanisms

In our recently published work, we reported on the mechanical behavior and deformation mechanisms of freestanding 3-D graphene foam.[52] The results of that study indicated that due to defects very few graphene branches actually bear any load, thereby indicating the potential was there for increased strengthening with the reduction of defects. The results of that study serve as a baseline for comparison with the results obtained in the present study for GrF-PLC hybrid. Nanoindentation was performed on the GrF-PLC hybrid in order to investigate the mechanical properties in compression, results are presented in **Table 1**. A 100 µm conospherical tip was used to indent the material to a depth of 750 nm. A typical indentation location is shown in the optical micrograph in **Figure 2**a. As previously stated, the thin layer of PLC allows the graphene foam to maintain its porous structure; hence indents were performed on both branches and nodes. The localized nature of nanoindentation yields information on the walls of the GrF-PLC hybrid, the properties of the bulk foam structure can be determined using a simple volume based relation first established by Gibson and Ashby given below as Equation (1),[53]

$$\frac{E^*}{E_s} = C_1\left(\frac{\rho^*}{\rho_s}\right)^2 ; C_1 = 1 \quad (1)$$

where the subscript "s" denotes the solid wall property, and the superscript "*" denotes the foam property.

The load-displacement curve in Figure 2b reveals that that the GrF-PLC hybrid has similar behavior to the previously reported pure graphene foam. The branch-node structure of the foam causes deformation to occur by both indentation of the foam wall as well by bending at the branch-node junctions. The load increases steadily under a mixed mode deformation process, where the branch bending is the primary mechanism, until about a depth of 600 nm. The slope then increases substantially as the deformation mechanism changes from branch bending to foam wall indentation.[52] After a critical depth, branch bending returns as the primary mechanism. This behavior is

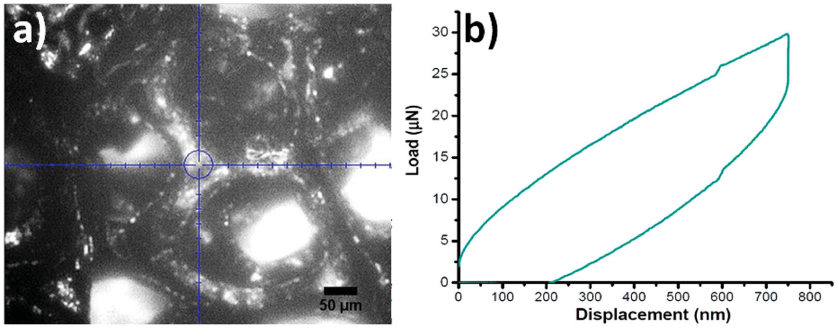

Figure 2. a) Optical image representative of typical nanoindentation test location. b) Characteristic nanoindentation curve for GrF-PLC hybrid.

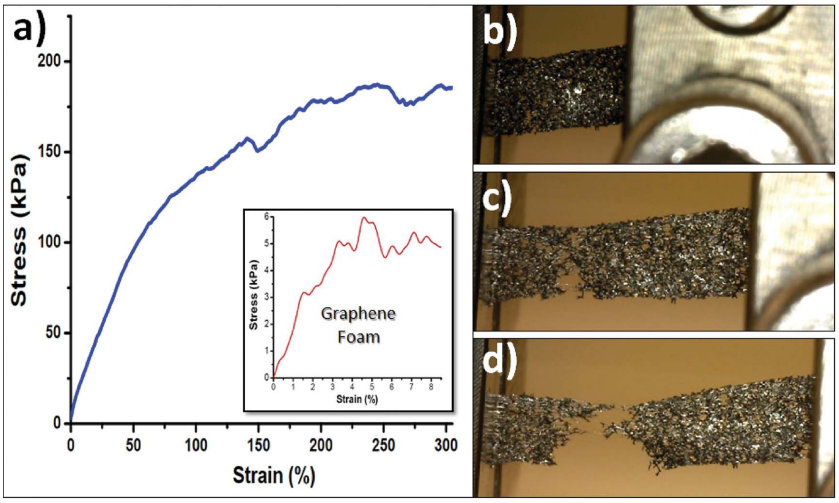

Figure 3. a) Characteristic stress–strain curve of GrF-PLC. Inset: Characteristic curve of pure graphene foam. b) GrF-PLC sample in tensile test setup. c) GrF-PLC sample in tension showing signs of necking. d) GrF-PLC after tensile failure, load prior to failure can be seen to be borne by a few high strength strands.

mirrored during the unloading portion of the curve. While the deformation mechanisms are similar, the compression strength of the GrF-PLC walls and hence the foam structure, are significantly higher than that of the pure graphene foam. The primary reason for strengthening in compression is due to the "healing" effect the PLC coating has on the graphene foam. The high wettability of PLC with the graphene foam allows it to fill preexisting microvoids and microcracks thereby providing increased resistance to elastic and plastic deformation.

The mechanical properties in tension were evaluated by macroscale tensile testing, these properties can be used to determine the foam wall properties by employing Equation (1). Results of macroscale tensile testing, shown in **Figure 3**, indicate that the addition of PLC dramatically increases the ductility and tensile strength of the GrF-PLC hybrid. Graphene foams typically fail at strains of about ≈8.5%, while the GrF-PLC hybrids typically reach values of ≈276% as shown in Figure 3a, an increase of about 3100%. Unlike the brittle failure response exhibited by the graphene foam, the GrF-PLC hybrid undergoes necking as seen in Figure 3c. During necking branches of GrF-PLC become aligned as is common in foam structures,[53] this is followed by the failure of individual low strength branches which correspond to the valleys in the stress–strain curves prior to failure. A few high strength branches continue to bear the load prior to failure as can be seen in Figure 3d. This results in the GrF-PLC hybrid scaffold having an ultimate tensile strength of ≈184 kPa, an increase of ≈3700% relative to the pure graphene foam scaffold. Using Equation (1) the elastic modulus of the GrF-PLC hybrid is calculated to be ≈52 GPa, a value substantially higher than that of PLC (≈81 MPa.[54] This exceptional high strength enables the utilization of a very porous structure, which is favorable for cell proliferation, without compromising the scaffold's mechanical performance. The substantially higher mechanical properties in tension relative to those in compression are expected as it was shown in our previous work that the high in-plane strength of graphene is only utilized in the foam structure during tension after branches become aligned with the loading direction.[52]

In order to further investigate the deformation mechanisms of GrF-PLC in situ tensile testing was conducted inside an SEM. The reinforcing effect of PLC can be clearly seen during tensile testing (Videos S3 and S4 in the Supporting Information show in situ tensile tests). An individual bridge of PLC can be seen under tension in **Figure 4**a, the same bridge in seen after being strained for 18 s in Figure 4b. The PLC bridges along with the excellent bonding with the graphene foam allows for branches to be elongated substantially before fracturing. PLC may also form high strength branches composed of multiple bridges as shown in Figure 4c, after 25 s of straining the branch has still not failed as each individual PLC bridge fails one by one as seen in Figure 4d.

To summarize, the addition of PLC can hence be seen to provide strength to the GrF-PLC scaffold in both compression and tension. The PLC provides dual strengthening mechanisms through i) defect healing and ii) PLC bridge formation. The excellent reinforcement effects originate from the excellent wettability between PLC and graphene foam. This high wettability enables the PLC to heal defects in the graphene foam by filling in branch discontinuities, microcracks, and microvoids. These cracks and discontinuities otherwise serve as stress concentrators which result in early branch failure and result in very few branches bearing loads. The filling of these voids with PLC enables more branches to participate in load bearing, thereby greatly enhancing strength. In addition to healing defects, the PLC serves as a fiber reinforcement due to the formation of PLC bridges that provide additional strength and ductility to the

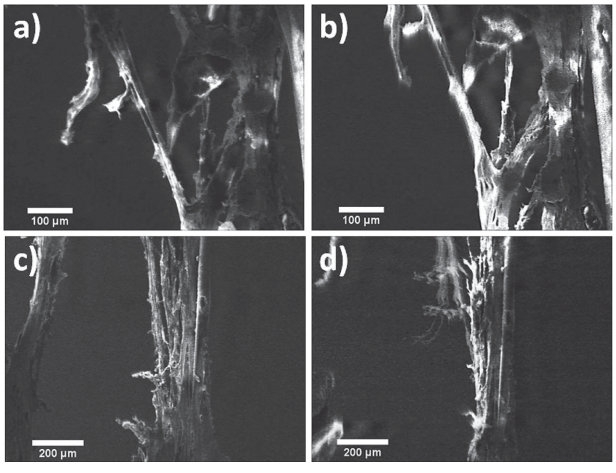

Figure 4. PLC reinforcing effect observed during in situ tensile testing. a) PLC bridge becomes stretched during tensile test. b) After 18 s, PLC bridge becomes stretched, enables foam branches to elongate without fracture. c) Branch composed of multiple PLC bridges under tension. d) After 25 s, PLC bridges become elongated and snap one by one, graphene foam branch at left has fractured.

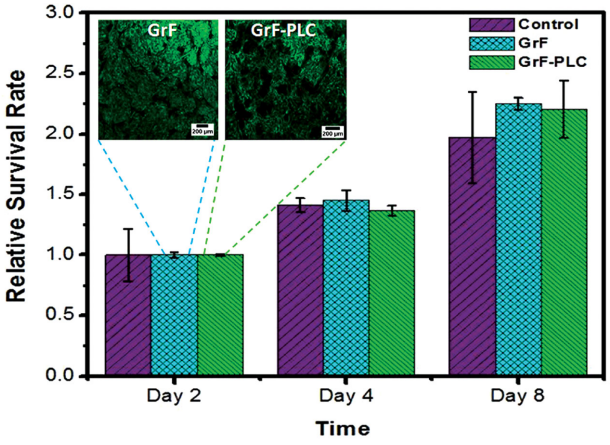

Figure 5. Relative survival of hMSCs in GrF and GrF-PLC scaffolds in comparison to hMSCs grown in a monolayer within a cell culture flask. Proliferation of hMSCs in the two scaffold environments was comparable to standard cell culture methods after 8 days of assessment. Insets show live-dead staining of hMSCs seeded on GrF and GrF-PLC scaffolds after 2 days, green indicates live cells, hardly any red dye (dead cells) is observed on either sample. One way ANOVA tests indicate no significant differences ($p > 0.05$) in survival rate among the GrF and GrF-PLC scaffolds or the control environment.

hybrid structure. The excellent wettability leads to the formation of a high strength interface with the foam which allows loads to be effectively transferred to the PLC bridges.

2.3. Cellular Studies

In order to validate the efficacy of the GrF-PLC for cartilage tissue engineering purposes, cellular studies are conducted using hMSCs. Previous efforts have demonstrated suitability of 3-D graphene foam for the culture of NSCs.[25,33] Here we first evaluate the survivability of hMSCs on the pure graphene foam and then assess the effect of adding the biocompatible copolymer PLC. Results of survivability of the hMSCs over a period of 8 days are shown in **Figure 5**. The results are normalized relative to the second day, where a value of 1.0 indicates that all cells have successfully survived in their new environment – either the graphene foam or the GrF-PLC scaffold. The results indicate that hMSCs survive on both the graphene foam and GrF-PLC scaffold just as they would in a controlled cell culture environment. The insets of Figure 5 show the "live-dead" staining of the cells (mitochondrial imaging is provided in Supporting Information, Figure S5), where the green dye indicates cells are alive, no red stains are observed as all cells have survived in both the graphene foam and GrF-PLC scaffold. Survival rate values for days 4 and 8 are above 1.0, this indicates that the cells not only survive but they have proliferated—i.e., they have grown and reproduced. It can be seen that for all days cells survive and proliferate to statistically equivalent ($F = 1$, $p > 0.05$) levels in both the GrF/GrF-PLC scaffold environments and the cell culture.

Imaging of the hMSCs in the graphene foam and GrF-PLC hybrid was conducted using SEM and fluorescence microscopy in order to assess any differences in cell growth due to

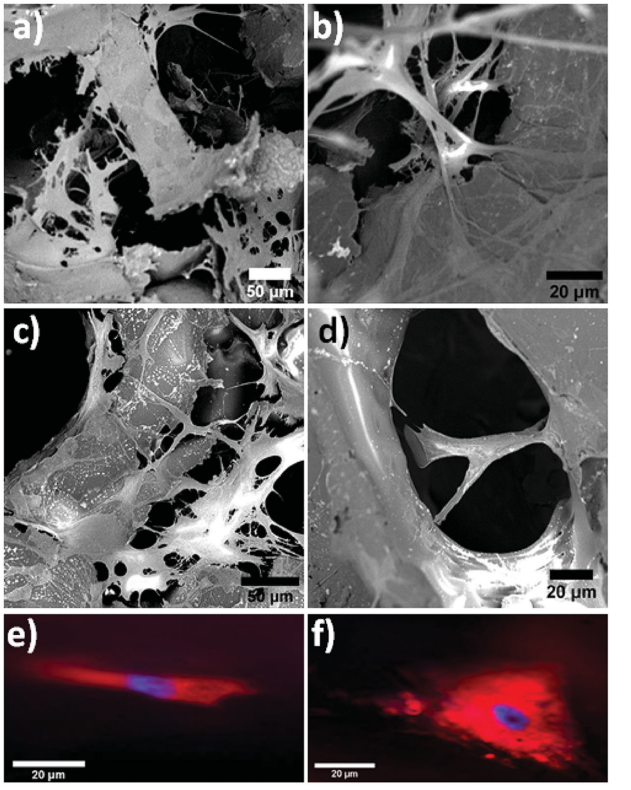

Figure 6. a,b) SEM images of graphene foam scaffold with human mesenchymal stem cells (hMSCs). c,d) SEM images of graphene foam-PLC hybrid scaffold with human mesenchymal stem cells (hMSCs). e) Fluorescence microscopy image of stem cells on graphene foam, cells appears severely stretched and thinned due to the graphene foam yielding under the cell induced stresses. f) Fluorescence microscopy images of stem cells on graphene foam-PLC scaffold, cells have a larger and more rounded morphology indicating normal growth.

the variations in scaffold composition and mechanical strength. **Figure 6** presents SEM and fluorescence images of the hMSCs in the graphene foam and GrF-PLC scaffolds after 28 days of growth in the stem cell media. The SEM images of hMSCs are comparable to those observed growing on high surface area micro-objects by Leferink et al.[55] The long strands seen in the images in Figure 6 are the hMSC cells; it can be seen that hMSCs grow in all directions, forming bridges across pores in the GrF and GrF-PLC structures. The porous networked structure is desirable for providing the cells an environment closer to that experienced in vivo, hence it is critical that cells do indeed grow through pores and form 3-D networks of cells during growth. Smaller spherical objects observed in the SEM images, also seen by Leferink et al.,[55] are believed to be products of the formation of ECM material; the presence of ECM indicates that the stem cells are metabolically active.

Fluorescence images in Figure 6d,e highlight the nucleus of individual stem cells in blue, and the surrounding cell plasma membrane in red. It can be seen that the nucleus and plasma membrane of the stem cells grown on GrF exhibit a highly elongated morphology as compared to those grown in the GrF-PLC scaffold. The hMSCs on the graphene foam become stretched and thinned likely because the foam is mechanically yielding.

As the cells adhere and grow onto the foam they induce strains on the foam, much the same way as substrates are strained during deposition of thin films and thermal spray coatings. The foam walls are not constrained as a substrate would be and the adhesion between cells and the foam is strong so that rather than debonding, the cell-induced tensile strains cause the graphene foam to become deformed. This causes the cells to be stretched and grow along the deformed foam. Signs of damage in the graphene foam can be seen in Figure 6a,b, the graphene foam has many jagged edges caused by mechanical deformation. The GrF-PLC scaffold in contrast was shown to have superior mechanical strength and hence it is able to support the cells without undergoing deformation, SEM images in Figure 6c,d show that the GrF-PLC scaffold retains a smooth morphology in the scaffold walls. The high strength GrF-PLC scaffold therefore provides a suitable structure for hMSCs to undergo normal growth.

2.4. Differentiation

Stem cells are pluripotent; hence the demonstration of feasibility of effective cell seeding and subsequent differentiation of hMSCs makes the GrF-PLC scaffold a potential candidate for many tissue engineering applications. As stated before, the GrF-PLC scaffold has several advantageous properties in particular, for musculoskeletal tissue engineering applications such as a lubricating surface, high surface area, and efficient energy dissipation. The hMSCs on the GrF and GrF-PLC scaffolds were cultured in a chondrogenic media for 28 days in order to induce differentiation into chondrocytes—the building blocks of cartilage tissue. Cartilage tissue can be characterized by the expression of type II collagen and aggrecan ECM protein. Analysis of the relative amounts of collagen and aggrecan in the samples after 28 days of culturing are done using immunostaining and subsequent quantification of the resulting stain intensities (**Figure 7**).

The presence of both aggrecan and type II collagen positive staining is seen throughout the graphene foam and GrF-PLC scaffold, thus indicating the successful differentiation of hMSCs into chondrocytes. Of particular importance, are the relative ratios of aggrecan to collagen present in the samples. Aggrecan is known to be a primary load-bearing component of cartilage ECM, hence making its presence critical for load bearing systems such as the human knee.[56–58] In healthy adult cartilage, the synthesis and degradation of aggrecan and other components of the cartilage ECM is self-regulated to ensure the proper balance needed for functionality.[57] Figure 7e shows that the ratio of aggrecan to collagen is higher in the pure graphene foam as compared to the GrF-PLC scaffold. It was seen that the pure graphene foam had less mechanical strength than the GrF-PLC scaffold. This results in the graphene foam undergoing deformation as de novo tissue grows, that initiates relatively larger transfer of loads onto the hMSCs. This constrains the cells into a compressed state which alters their shape by stretching and thinning (Figure 6e). The altered morphology subsequently initiates a cascade of cell signaling events to promote overproduction of Aggrecan ECM protein by hMSCs. It is important to note here that a major function of aggrecan is indeed to resist loads in compression.[59]

On the other hand, the GrF-PLC foam retains a more dilated hMSC structure (Figure 6f) which serves to reduce hMSC-derived aggrecan synthesis. At 28 day post-culture, the engineered tissues are primarily supported by the GrF-PLC scaffold with minimal loads transferred onto the cells. Thus, in contrast to the graphene foam alone, in the GrF-PLC hybrids, resistance to loading via overproduction of hMSC-derived aggrecan is not necessary since the scaffold bears the bulk of the loading. We note however that despite lower levels of aggrecan, cells within the GrF-PLC-seeded samples were found to be healthy (Figure 5) and exhibited relatively robust expression of type II collagen and negligible expression of type I collagen (Figure 7e) demonstrating support for the articular cartilage phenotype.

Evidence of positive collagen type II staining was evident in both the hMSC-seeded graphene-only foam (Figure 7b) and hMSC-seeded graphene foam-PLC composite scaffolds (Figure 7d). The intensity of staining was found to be slightly higher in the graphene foam-PLC hybrid as compared to the

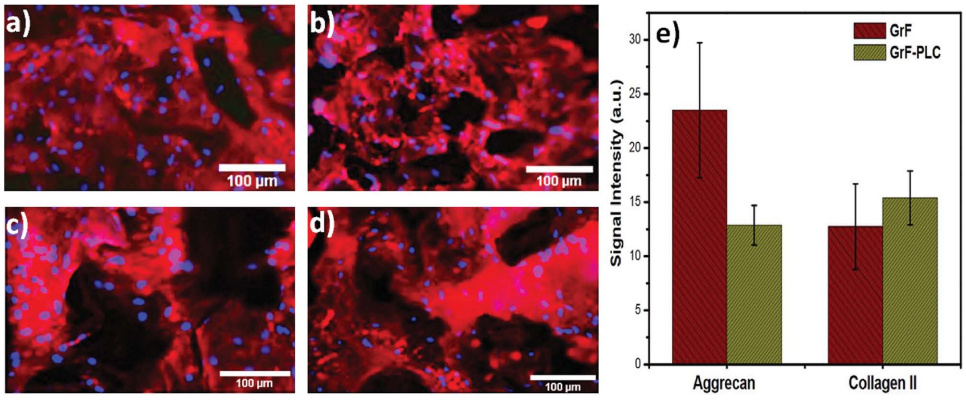

Figure 7. a) Aggrecan immunostaining on graphene foam scaffold. b) Type II collagen immunostaining on graphene foam scaffold. c) Aggrecan immunostaining on graphene foam-PLC hybrid scaffold. d) Type II collagen immunostaining on graphene foam-PLC hybrid scaffold. e) Signal intensities of aggrecan and type II collagen taken from various sample sites on graphene foam and graphene foam-PLC hybrid scaffolds. HMSCs can be seen to have successfully differentiated in the chondrogenic media. T-tests indicate statistically significant differences in aggrecan ($p < 0.05$) but not in type II collagen ($p > 0.05$). Type I collagen expression was found to be negligible in both groups.

graphene foam counterpart but the difference was not significant ($p > 0.05$). Nonetheless, the robust positive staining of collagen II in combination with the demonstrated aggrecan synthesis by the samples (Figure 7a,c) provides evidence that both scaffold groups (hMSC-seeded graphene-only foam and hMSC-seeded graphene foam-PLC composite) continue to support hMSC differentiation along a healthy chondrogenic signaling pathway. Specifically, the chondrogenic media that was utilized while proprietary, is likely to have contained sufficient concentration of the critical cytokine, transforming growth factor-beta 1 (TGF-β1), for inducing differentiation of hMSCs to chondrocytes within the in vitro cultured, graphene-based scaffold environments.[60] This being the case, we believe that the signaling pathway for hMSC differentiation is TGF-β1-mediated. It is well-known that the TGF-β1 pathway initiates via its receptor linkage with the activin-like kinase 1 (ALK 1) transmembrane protein; following this, activation of the intracellular Smad 2–3 signaling molecule occurs, which in turn leads to the promotion of the articular cartilage phenotype.[61]

3. Conclusions

A high strength biocompatible scaffold is synthesized by dipping a graphene foam into a liquid solution of the copolymer PLC. The excellent wettability of PLC on graphene foam enables the PLC to form a thin uniform coating over the graphene foam. The high wettability allows the PLC to fill voids and defects present in the graphene foam. The healing of defects in conjunction with the formation of PLC bridges leads to enhanced strength and ductility in the GrF-PLC scaffold. Nanoindentation and macroscale tensile testing shows the increase in strength in both compression and tension at multiple scales. The effectiveness of PLC bridges bearing load is observed directly via in situ tensile testing in an SEM.

Cellular studies conducted on both graphene foam and GrF-PLC scaffolds demonstrate the ability of hMSCs to survive and proliferate throughout both scaffolds. The higher strength of the GrF-PLC scaffold enables the hMSCs to grow normally without undergoing large deformations. The pure graphene foam does not have sufficient strength to withstand cell-induced strains and leads to hMSCs growing with a highly elongated morphology (Figure 6e). The change in cell shape causes aggrecan ECM protein overproduction. By contrast, the cells within the GrF-PLC specimens retain their unconstrained shape (Figure 6f). Subsequently significantly lower ($p < 0.05$) aggrecan content in the GrF-PLC specimens is found compared to its graphene foam-alone counterparts. However, cells within the hybrid material are still able to express slightly higher levels of type II collagen and negligible levels of type I collagen, thereby indicating that GrF-PLC scaffolds permit chondrogenesis of hMSCs (Figure 7e). Since cartilage is load bearing and its ECM constituents are self-regulated, it may be important for the scaffold material to bear the bulk of the loads from the de novo tissues. This is so that in situ cellular proliferation and migration as well as ECM deposition can occur in timescales mimicking normal developmental processes, while cellular overproduction of matrix components is avoided. As mentioned earlier, adequate cell distribution and ECM layering within the treatment space is critical to long-term success. We demonstrate here that GrF-PLC has the ability to serve as a principal support structure for hMSC-derived engineered tissues resulting in minimal imposition of loads onto the cells thereby reducing their burden to secrete aggrecan, a primary component of articular cartilage ECM. Thus we conclude that the superior mechanical properties of GrF-PLC scaffolds such as augmented strength and ductility and the ability to support stem cell viability and differentiation make it a suitable candidate for musculoskeletal tissue engineering applications, such as the growth of cartilage ECM.

4. Experimental Section

Materials: The graphene foam used in this study was procured from Graphene Laboratories (Calverton, NY, USA). The graphene foam is synthesized by growing graphene on a nickel foam template. The nickel template is then etched away, leaving behind only a free standing 3D graphene foam structure. The starting copolymer of polylactic acid and poly-ε-caprolactone (PLC) in 70:30 molar ratio was procured from Purac Biomaterials (Lincoln, IL, USA). The PLC solution was prepared by mixing 1 g of PLC with 20 mL of acetone in a 50 mL beaker; the mixture was stirred for 20 min using a magnetic stirring. Wetting angles measurements between the graphene foam and either PLC or water were conducted using a DM-CEI Contact Angle Meter (Kyowa Interface Science Co., JAPAN). Each droplet of PLC or water had a volume of approximately 2 µL. Contact angles were calculated with the aid of Kyowa FAMAS software. Pure graphene foam was then dipped in the PLC solution for a set amount of time; the GrF-PLC scaffold found to have the optimal PLC coating was dipped in PLC of 5 s. The morphology of the GrF-PLC scaffolds was characterized using a FEI PHENOM scanning electron microscope with an operating voltage of 5 kV.

Mechanical Characterization: A TI-900 Triboindenter (Hysitron, Minneapolis, MN, USA) was used to conduct nanoindentation experiments. A 100 µm radius conospherical tip was used to perform displacement-controlled indentations with a depth of 750 nm. The load cycle consisted of a 10 s ramp to 750 nm, following by a 3 s hold at 750 nm, and finally a 10 s unloading. The elastic modulus of the graphene foam and GrF-PLC scaffold were evaluated using the Oliver–Pharr method.[62] Tensile testing was performed using an Electroforce 3200 tensile tester (BOSE, Eden Prairie, MN, USA) equipped with a 10 N load cell. The crosshead speed was 0.05 mm s^{-1} and the maximum displacement was 12 mm. The tensile specimens had dimensions of approximately 16 mm gauge length, 5 mm width, and 200 µm thickness. In situ tensile testing was performed inside a JEOL JIB-4500 MultiBeam SEM-FIB using an MTI SEM tester1000 microload frame. The crosshead speed used during in situ tests was also 0.05 mm s^{-1}. In situ testing was used for the sole purpose of observing deformation mechanisms under tensile loading.

HMSC Growth and Characterization: Human bone marrow derived mesenchymal stem cells (ScienCell, Carlsbad, CA, USA) were seeded onto Poly D-lysine coated T-75 flasks (Fisher Scientific, Pittsburg, PA, USA). The cells were cultured in the AdvanceSTEM Mesenchymal Stem Cell Expansion Kit (Thermo Scientific, Waltham, WA) until passage three. Cell proliferation on the scaffold samples was determined using the sulforhodamine B (SRB) Viability/Cytotoxity Assay Kit (Vitro Vivo Biotechnology, Rockville, MD)) which is based on the measurement of viable cellular protein colorimetrically. HMSCs were seeded on GrF and GrF-PLC scaffolds of size 5 mm^2 with a cell density of 105 cells mL^{-1}. They were kept in rotisserie for 24 h and then the samples were transferred in 24 well plates in the fresh stem cell media to allow the cells to expand. SRB assay was performed for day 2, day 4, and day 8 on three samples for each day each time period and results were analyzed. To perform the SRB assay, first the cells were fixed to the bottom of the sample using trichloroacetic acid which acted as the fixative. Then the cells were stained using the SRB dye. The unbounded

dye was removed using 1% acetic acid. The dye bounded to the cellular protein was extracted using 10×10^{-3} M Trizma base and the absorbance was measured at a wavelength of 565 nm in BioTek Plate Reader (Biotek Instruments, Inc, Winooski, Vermont). A Live-Dead assay using Calcein AM/Ethidium homodimer (Life Technologies) staining was applied in order to assess the viability of cells on the scaffolds. In brief, samples from these two groups were stained with Calcein AM and Ethidium homodimer in phospate buffer saline (PBS) solution and incubated for 30 min. Next, they were washed three times with PBS solution to remove the background fluorescence and subsequently visualized under the fluorescent microscope (Olympus IX81, Olympus IX81, Olympus America Inc., Miami FL) at excitation and emission wavelengths of 468 and 568 nm, respectively. Cell viability was subsequently computed for day 2 by counting cells on the three images of each group (ImageJ software, NIH, Bethesda, MD) and calculating the ratio of live cells (green dots) to the sum of live and dead cells (red dots), results of subsequent days were normalized with respect to day 2 measurements. To study the morphology of HMSC seeded on GrF and GrF-PLC scaffolds, live mitochondrial and nuclear imaging of cells was performed using the Live Mitochondrial and Nuclear Labeling Kit (Invitrogen). The GrF and GrF-PLC scaffold samples seeded with hMSCs were incubated with 200×10^{-9} M MitoTracker Red and 5×10^{-6} M Hoechst dye in media for 15 min at 370 °C. When labeling was completed the excess labeling solution was removed by washing with PBS twice. The samples were observed under fluorescence microscope (Olympus IX 81). Samples with cells were also observed with SEM, cells were fixed with chilled ethanol prior to SEM analysis.

Immunohistochemical Studies: HMSC seeded on GrF and GrF-PLC was allowed to differentiate into chondrocytes by culturing them in chondrogenic media (HyClone AdvanceSTEM Chondrogenic Differentiation Medium, Catalog No. SH3088902, Fisher Scientific, Pittsburgh, PA) for 28 d. After 28 d of culture, the graphene and PLC coated graphene were subjected to immunohistochemical studies to test for the presence of collagen types I and II and aggrecan. Briefly, the samples were removed from the well plate in which they were cultured, washed with PBS, fixed with 10% formalin for 2 h at room temperature, and washed again three times with PBS. All sections were subjected to a 2 mg mL^{-1} hyaluronidase (Fisher Scientific) treatment for 30 min at 370 °C to enhance the binding of the primary antibodies. Samples were then subjected to antigen retrieval process using sodium citrate buffer (10×10^{-3} M sodium citrate, 0.05% tween 20, pH 6.0) at 950–1000 °C for 3 min. For the samples testing for aggrecan, the sections were reduced with 10×10^{-3} M dithiothreitol in 50×10^{-3} M tris HCl, 200×10^{-3} M sodium chloride, pH 7.4, for 2 h at 37 °C. Then the samples were further alkylated by placing them in 40×10^{-3} M iodoacetic acid in PBS for 1 h at 37 °C. After the alkylation was done, samples were washed in PBS for 5 min. After this, all samples were blocked using 2.5% goat serum (Vector Laboratories) for 1 h at room temperature. Excessive blocking buffer was rinsed with a gentle stream of wash buffer solution (1000 mL of PBS and 0.5 mL of tween 20). After serum blocking, primary antibodies mouse anti-pro-collagen I (SP1.D8), anti-collagen II (CIIC1), and anti-aggrecan link protein (9/30/8-A-4) purchased from the Developmental Studies Hybridoma Bank (University of Iowa, Iowa City, IA) were diluted in 1% goat serum to a concentration of 5 μg mL^{-1} and were added to the sections and incubated overnight at 4 °C. Sections were then incubated with Goat polyclonal Secondary Antibody to Mouse IgG – H&L Cy3-conjugated (Abcam, Cambridge, MA) diluted to 1/50 to the original concentration of 500 μg at 0.5 mg mL^{-1} for 45 min at 37 °C. Sections were counter stained with Mounting Media with DAPI (Vector Laboratories, Burlingame, CA) and observed under the fluorescence microscope ((Olympus America, Melville, NY). In order to quantify the level of aggrecan and type II collagen gene expression, images were selected ($n = 4$/group) and signal intensity measured (ImageJ).

Statistics: Statistical analyses were conducted on cell viability and immunohistochemical studies to assess whether significant trends were present. One way analysis of variance (ANOVA) tests were conducted on the cell survival rates for each time period to access whether there was a statistically significant survival rate between the GrF scaffold, GrF-PLC scaffold, or control environment for a given time period. F values near 1.0 and $p > 0.05$ indicated differences in survival rate were not significant. T-tests were conducted to access whether there was a statistically significant difference of either aggrecan or type II collagen in the GrF and GrF-PLC scaffolds. A value of $p < 0.05$ was taken to indicate a statistically significant difference in value.

Supporting Information

Supporting Information is available from the Wiley Online Library or from the author.

Acknowledgements

The authors would like to thank Dr. Norman Munroe for extending the use of Contact Angle Meter equipment. The assistance of Mr. Vishal Musaramthota in performing wetting angle experiments is greatly appreciated. The authors acknowledge support from the Advanced Materials Engineering Research Institute (AMERI) at FIU for providing and maintaining electron microscopy facilities.

Received: March 4, 2015
Revised: April 21, 2015
Published online: May 20, 2015

[1] W. Wei, X. Qu, *Small* **2012**, *8*, 2131.
[2] C. N. R. Rao, A. K. Sood, R. Voggu, K. S. Subrahmanyam, *J. Phys. Chem. Lett.* **2010**, *1*, 572.
[3] C. Soldano, A. Mahmood, E. Dujardin, *Carbon* **2010**, *48*, 2127.
[4] W. Choi, I. Lahiri, R. Seelaboyina, Y. S. Kang, *CRC Cr. Rev. Sol. State* **2010**, *35*, 52.
[5] A. A. Balandin, S. Ghosh, W. Bao, I. Calizo, D. Teweldebrhan, F. Miao, C. N. Lau, *Nano Lett.* **2008**, *8*, 902.
[6] C. Lee, X. Wei, J. W. Kysar, J. Hone, *Science* **2008**, *321*, 385.
[7] I. W. Frank, D. M. Tanenbaum, A. M. Van der Zande, P. L. McEuen, *J. Vac. Sci. Technol.* **2007**, *B25*, 2558.
[8] L. Gong, I. A. Kinloch, R. J. Young, I. Riaz, R. Jalil, K. S. Novoselov, *Adv. Mater.* **2010**, *22*, 2694.
[9] Q. Lu, M. Arroyo, R. Huang, *J. Phys. D Appl. Phys.* **2009**, *42*, 102002.
[10] C. Liu, J. Yang, Y. Tang, L. Yin, H. Tang, C. Li, *Colloid Surf. A* **2015**, *468*, 10.
[11] Y. A. Samad, Y. Li, A. Schiffer, S. M. Alhassan, K. Liao, *Small* **2015**, DOI: 10.1002/smll.201403532.
[12] Y. S. Moon, D. Kim, G. Lee, S. Y. Hong, K. K. Kim, S. M. Park, J. S. Ha, *Carbon* **2015**, *81*, 29.
[13] A. Bello, F. Barzegar, D. Momodu, J. Dangbegnon, F. Taghizadeh, M. Fabiane, N. Manyala, *J. Power Sources* **2015**, *273*, 305.
[14] G. Zhou, L. Li, C. Ma, S. Wang, Y. Shi, N. Koratkar, W. Ren, F. Li, H.-M. Cheng, *Nano Energy* **2015**, *11*, 356.
[15] X. Zhou, Z. Bai, M. Wu, J. Qiao, Z. Chen, *J. Mater. Chem. A* **2015**, *3*, 3343.
[16] S. Chabi, C. Peng, Z. Yang, Y. Xia, Y. Zhu, *RSC Adv.* **2015**, *5*, 3999.
[17] J. Liu, J. Wang, D. Li, F. Xi, J. Wang, E. Wang, *Bio Sens. Bioelectron.* **2015**, *65*, 281.
[18] R. Xu, Y. Lu, C. Jiang, J. Chen, P. Mao, G. Gao, L. Zhang, S. Wu, *ACS Appl. Mater Inter.* **2014**, *6*, 13455.
[19] J. Jia, X. Sun, X. Lin, X. Shen, Y.-W. Mai, J.-K. Kim, *ACS Nano* **2014**, *8*, 5774.
[20] S.-H. Lee, J.-H. Jung, I.-K. Oh, *Small* **2014**, *10*, 3880.
[21] Y. Li, J. Chen, L. Huang, C. Li, J.-D. Hong, G. Shi, *Adv. Mater.* **2014**, *26*, 4789.

[22] Z. Chen, C. Xu, C. Ma, W. Ren, H.-M. Cheng, *Adv. Mater.* **2013**, *25*, 1296.
[23] W. Chen, Z. Fan, G. Zeng, Z. Lai, *J. Power Sources* **2013**, *225*, 251.
[24] E. Singh, Z. Chen, F. Houshmand, W. Ren, Y. Peles, H.-M. Cheng, N. Koratkar, *Small* **2013**, *9*, 75.
[25] N. Li, Q. Zhang, S. Gao, Q. Song, R. Huang, L. Wang, L. Liu, J. Dai, M. Tang, G. Cheng, *Sci. Rep.* **2013**, *3*, 1604.
[26] M. Zhou, T. Lin, F. Huang, Y. Zhong, Z. Wang, Y. Tang, H. Bi, D. Wan, J. Lin, *Adv. Funct. Mater.* **2013**, *23*, 2263.
[27] X. Dong, X. Wang, L. Wang, H. Song, H. Zhang, W. Huang, P. Chen, *ACS Appl. Mater. Inter.* **2012**, *4*, 3129.
[28] X. Cao, Y. Shi, W. Shi, G. Lu, X. Huang, Q. Yan, Q. Zhang, H. Zhang, *Small* **2011**, *7*, 3163.
[29] F. Yavari, Z. Chen, A. V. Thomas, W. Ren, H.-M. Cheng, N. Koratkar, *Sci. Rep.* **2011**, *1*, 166.
[30] T. R. Nayak, H. Andersen, V. S. Makam, C. Khaw, S. Bae, X. Xiangfan, P.-L. R. Ee, J.-H. Ahn, B. H. Hong, G. Pastorin, B. Ozyilmaz, *ACS Nano* **2011**, *5*, 4670.
[31] S. Y. Park, J. Park, S. H. Sim, M. G. Sung, K. S. Kim, B. H. Hong, S. Hong, *Adv. Mater.* **2011**, *23*, H263.
[32] Y. Wang, W. C. Lee, K. K. Manga, P. K. Ang, J. Lu, Y. P. Liu, C. T. Lim, K. P. Loh, *Adv. Mater.* **2012**, *24*, 4285.
[33] Q. Song, Z. Jiang, N. Li, P. Liu, L. Liu, M. Tang, G. Cheng, *Biomaterials* **2014**, *35*, 6930.
[34] Z. Chen, W. Ren, L. Gao, B. Liu, S. Pei, H.-M. Cheng, *Nat. Mater.* **2011**, *10*, 424.
[35] H.-B. Zhang, Q. Yan, W.-G. Zheng, H. Zhixian, Z.-Z. Yu, *ACS Appl. Mater. Inter.* **2011**, *3*, 918.
[36] Y. Zhao, J. Liu, Y. Hu, H. Cheng, C. Hu, C. Jiang, L. Jiang, A. Cao, L. Qu, *Adv. Mater.* **2013**, *25*, 591.
[37] C. Wu, X. Huang, X. Wu, R. Qian, P. Jiang, *Adv. Mater.* **2013**, *25*, 5658.
[38] I.-C. Liao, F. T. Moutos, B. T. Estes, X. Zhao, F. Guilak, *Adv. Funct. Mater.* **2013**, *23*, 5833.
[39] A. Nieto, D. Lahiri, A. Agarwal, *Mater. Sci. Eng. A-Struct.* **2013**, *582*, 338.
[40] Z. Xu, X. Shi, W. Zhai, J. Yao, S. Song, Q. Zhang, *Carbon* **2014**, *67*, 168.
[41] T. Ramanathan, A. A. Abdala, S. Stankovich, D. A. Dikin, M. Herrera-Alonso, R. D. Piner, D. H. Adamson, H. C. Schniepp, X. Chen, R. S. Ruoff, S. T. Nguyen, I. A. Aksay, R. K. Prud'Homme, L. C. Brinson, *Nat. Nanotechnol.* **2008**, *3*, 327.
[42] M. A. Rafiee, J. Rafiee, Z. Wang, H. Song, Z. Z. Yu, N. Koratkar, *ACS Nano* **2009**, *3*, 3884.
[43] D. Lahiri, S. Das, W. Choi, A. Agarwal, *ACS Nano* **2012**, *6*, 3992.
[44] A. Nieto, D. Lahiri, A. Agarwal, *Scr. Mater.* **2013**, *69*, 678.
[45] M. Belmonte, C. Ramirez, J. Gonzalez-Julian, J. Schneider, P. Miranzo, M. I. Osendi, *Carbon* **2013**, *61*, 431.
[46] L. Wang, W. Ma, R. A. Gross, S. P. McCarthy, *Polym. Degrad. Stabil.* **1998**, *59*, 161.
[47] R. Dua, J. Centeno, S. Ramaswamy, *J. Biomed. Mater. Res. B* **2014**, *102*, 922.
[48] N. T. Khanarian, J. Jiang, L. Q. Wan, V. C. Mow, H. H. Lu, *Tissue Eng. Pt. A* **2012**, *18*, 533.
[49] S. Ramaswamy, M. C. Uluer, S. Leen, P. Bajaj, K. W. Fishbein, R. G. Spencer, *Tissue Eng. Pt. C-Meth* **2008**, *14*, 243.
[50] D. A. Wang, C. G. Williams, Q. Li, B. Sharma, J. H. Elisseeff, *Biomaterials* **2003**, *24*, 3969.
[51] C. G. Williams, T. K. Kim, A. Taboas, A. Malik, P. Manson, J. Elisseeff, *Tissue Eng.* **2003**, *9*, 679.
[52] A. Nieto, B. Boesl, A. Agarwal, *Carbon* **2015**, *85*, 299.
[53] L. J. Gibson, M. F. Ashby, in *Cellular Solids – Structures and Properties* (Eds. D. R. Clark, S. Suresh, I. M. Ward), Cambridge University Press, Cambridge, UK **1997**, pp 175–281.
[54] D. Lahiri, F. Rouzaud, T. Richard, A. K. Keshri, S. R. Bakshi, L. Kos, A. Agarwal, *Acta Biomater.* **2010**, *6*, 3524.
[55] A. Leferink, D. Schipper, E. Arts, E. Vrij, N. Rivron, M. Karperien, K. Mittmann, C. Van Blitterswijk, L. Moloni, R. Truckenmuller, *Adv. Mater.* **2014**, *26*, 2562.
[56] C. Kiani, L. Chen, Y. J. Wu, A. J. Yee, B. B. Yang, *Cell Res.* **2002**, *12*, 19.
[57] J. R. Matyas, P. F. Ehlers, D. Huang, M. E. Adams, *Arthritis Rheum.* **1999**, *42*, 993.
[58] S. Roberts, J. Menage, L. J. Sandell, E. H. Evans, J. B. Richardson, *Knee* **2009**, *16*, 398.
[59] P. Roughley, D. Martens, J. Rantakokko, M. Alini, F. Mwale, J. Antoniou, *Eur. Cell. Mater.* **2006**, *11*, 1.
[60] L. A. Solchaga, K. J. Penick, J. F. Welter, *Mol. Bio.* **2011**, *698*, 253.
[61] E. Mariani, L. Pulsatelli, A. Facchini, *Int. J. Mol. Sci.* **2014**, *15*, 8667.
[62] W. C. Oliver, G. M. Pharr, *J. Mater. Res.* **1992**, *7*, 1564.